PROCEEDINGS OF SPIE

SPIEDigitalLibrary.org/conference-proceedings-of-spie

The evolution of structure and feedback with Arcus

Laura W. Brenneman, Randall K. Smith, J. Bregman, J. Kaastra, N. Brickhouse, et al.

Laura W. Brenneman, Randall K. Smith, J. Bregman, J. Kaastra, N. Brickhouse, R. Allured, A. Foster, S. Wolk, J. Wilms, L. Valencic, R. Willingale, C. Grant, M. Bautz, R. Heilmann, D. Huenemoerder, E. Miller, M. Nowak, M. Schattenburg, N. Schulz, V. Burwitz, K. Nandra, J. Sanders, J. Bookbinder, R. Petre, A. Ptak, A. Smale, D. Burrows, K. Poppenhaeger, E. Costantini, C. DeRoo, R. McEntaffer, R. Mushotzky, J. M. Miller, P. Temi, "The evolution of structure and feedback with Arcus," Proc. SPIE 9905, Space Telescopes and Instrumentation 2016: Ultraviolet to Gamma Ray, 99054P (18 July 2016); doi: 10.1117/12.2231193

SPIE.

Event: SPIE Astronomical Telescopes + Instrumentation, 2016, Edinburgh, United Kingdom

The evolution of structure and feedback with *Arcus*

Laura W. Brenneman*[a], Randall K. Smith[a], J. Bregman[b], J. Kaastra[c], N. Brickhouse[a], R. Allured[a], A. Foster[a], S. Wolk[a], J. Wilms[d], L. Valencic[e,f], R. Willingale[g], C. Grant[h], M. Bautz[h], R. Heilmann[h], D. Huenemoerder[h], E. Miller[h], M. Nowak[h], M. Schattenburg[h], N. Schulz[h], V. Burwitz[i], K. Nandra[i], J. Sanders[i], J. Bookbinder[j], R. Petre[d], A. Ptak[d], A. Smale[d], D. Burrows[k], K. Poppenhager[l], E. Costantini[c], C. DeRoo[m], R. McEntaffer[m], R. Mushotzky[n], J.M. Miller[b], P. Temi[j]

[a]Smithsonian Astrophysical Observatory, 60 Garden St., Cambridge, MA USA 02138; [b]University of Michigan, Department of Astronomy, 500 Church St., Ann Arbor, MI USA 48109-1042; [c]SRON, Sorbonnelaan 2, 3584 CA Utrecht, Netherlands; [d]Dr. Karl-Remeis-Sternwarte, Astronomisches Institut der Universität Erlangen-Nürnberg, Sternwartstr. 7, 96049 Bamberg, Germany; [e]Johns Hopkins University, Department of Physics & Astronomy, Bloomberg Center for Physics and Astronomy, Room 366, 3400 N. Charles Street, Baltimore, MD USA 21218; [f]NASA/GSFC, Code 662, Greenbelt, MD USA 20771; [g]Department of Physics & Astronomy, University of Leicester, University Road, Leicester, LE1 7RH, United Kingdom; [h]Massachusetts Institute of Technology, 70 Vassar Str., Bldg 37, NE80-6075, Cambridge, MA USA 02139; [i]Max-Planck-Institut für extraterrestrische Physik, Giessenbachstrasse , 85748 Garching, Germany; [j]NASA/Ames Research Center, Moffett Field, CA USA 94035; [k]Pennsylvania State University, Dept. of Astronomy & Astrophysics, 517 Davey Lab, University Park, PA USA 16802; [l]Queen's University Belfast, School of Mathematics and Physics, University Road, Belfast, BT7 1NN, Northern Ireland, UK; [m]Department of Physics and Astronomy, 203 Van Allen Hall, The University of Iowa, Iowa City, IA USA 52242-1479; [n]Department of Astronomy, University of Maryland, College Park, MD USA 20742-2421.

ABSTRACT

Arcus is a NASA/MIDEX mission under development in response to the anticipated 2016 call for proposals. It is a free-flying, soft X-ray grating spectrometer with the highest-ever spectral resolution in the 8-51 Å (0.24 – 1.55 keV) energy range. The *Arcus* bandpass includes the most sensitive tracers of diffuse million-degree gas: spectral lines from O VII and O VIII, H- and He-like lines of C, N, Ne and Mg, and unique density- and temperature-sensitive lines from Si and Fe ions. These capabilities enable an advance in our understanding of the formation and evolution of baryons in the Universe that is unachievable with any other present or planned observatory. The mission will address multiple key questions posed in the Decadal Survey[1] and NASA's 2013 Roadmap[2]: How do baryons cycle in and out of galaxies? How do black holes and stars influence their surroundings and the cosmic web via feedback? How do stars, circumstellar disks and exoplanet atmospheres form and evolve? *Arcus* data will answer these questions by leveraging recent developments in off-plane gratings and silicon pore optics to measure X-ray spectra at high resolution from a wide range of sources within and beyond the Milky Way. CCDs with strong *Suzaku* heritage combined with electronics based on the *Swift* mission will detect the dispersed X-rays. *Arcus* will support a broad astrophysical research program, and its superior resolution and sensitivity in soft X-rays will complement the forthcoming *Athena* calorimeter, which will have comparably high resolution above 2 keV.

Keywords: Large-scale structure; Active galaxies; Stars; Accretion; Outflows; X-rays; Spectroscopy; Gratings.
*email: lbrenneman@cfa.harvard.edu; phone: 1-617-496-9327.

Space Telescopes and Instrumentation 2016: Ultraviolet to Gamma Ray, edited by
Jan-Willem A. den Herder, Tadayuki Takahashi, Marshall Bautz, Proc. of SPIE Vol. 9905, 99054P
 · doi: 10.1117/12.2231193

1. STRUCTURE FORMATION

1.1 Galaxy Groups, Clusters, and the Cosmic Web

Structure formation naturally results in the production of hot gas (10^5-10^8 K) on the scales of galaxy groups and clusters, galactic halos, and the collapsing intergalactic filaments that comprise the cosmic web[3,4,5,6]. This gas accounts for roughly half of the baryons in the Universe, and its properties encode vital information about the formation and evolution of large-scale structure (LSS). This process is multi-step: the formation of galaxies produces a large number of massive stars and supernovae, along with a central supermassive black hole (SMBH). Feedback from these sources (see §2, §3) heats the accreting halo gas in different ways, but ultimately all of the energy and metals expelled through feedback are incorporated into the larger reservoir of the Warm-Hot Intergalactic Medium (WHIM). *Planck* observations support this picture, as large reservoirs of hot gas must surround massive galaxies, galaxy groups and clusters to account for the observed Sunyaev-Zel'dovich (S-Z) signal[7]. Processes central to galaxy and structure formation determine the spatial distribution, mass, temperature and chemical abundance of the WHIM gas. In the absence of direct observations of this gas, however, the relative roles of these feedback processes are largely unconstrained. *Arcus* will measure the thermodynamical state and composition of hot gas in the intergalactic medium (IGM) and interstellar medium (ISM) via absorption features from dominant ions in the plasma.

The study of this WHIM gas is much richer than searching for missing baryons; it is critical to our understanding of the formation and evolution of galaxies and larger structures in the Universe. The evolution of cold dark matter is straightforward, as it is the gravitational response to variations in the density and distribution of primordial matter in the Universe. In cosmological simulations, the collapse of dark matter filaments is governed only by gravity, but the gaseous component undergoes shocks, heating the gas to WHIM temperatures[8]. Intersecting cosmic filaments form nascent galaxy groups and clusters that grow through continued inflow in connective filaments (Fig. 1). The galaxy groups and clusters eventually become virialized, but they are difficult to study in emission at core distances greater than about half the virial radius[9,10,11]. The dark matter density follows an NFW profile ($n_{DM} \sim r^{-2.8}$ in the outer parts of galaxies and clusters), while the hot gas density near galaxies is flatter ($n_{gas} \sim r^{-1.5}$, equivalent to $\beta = 1/2$)[29], but the profile of the hot gas far from the core is unknown.

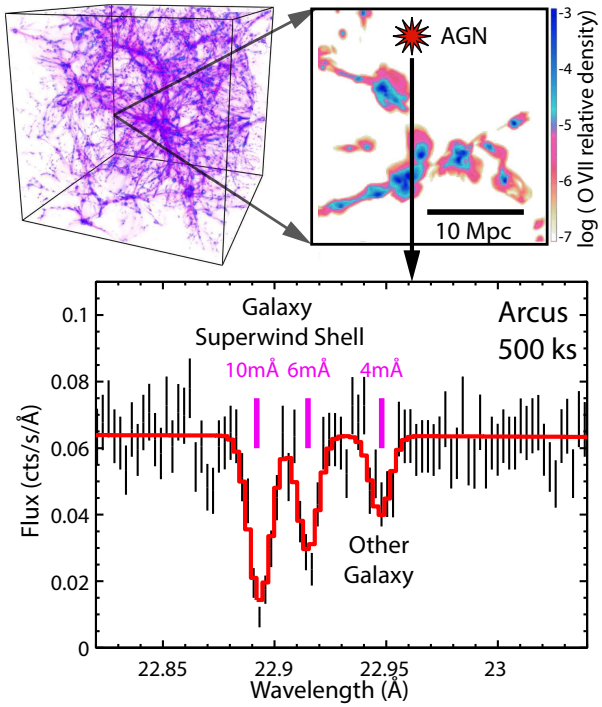

Figure 1. An LSS simulation, where dark matter fluctuations drive the baryonic matter into galaxy groups, clusters and filaments. The redshifted O VII absorption lines reveal the physical properties – e.g., temperature, velocity – of intervening gas along typical lines of sight.

Supernovae and feedback from active galactic nuclei (AGN) also combine to produce heavy elements from carbon through iron and distribute them into the WHIM. These metals produce the WHIM absorption lines, revealing not only the gas distribution and mass, but also its enrichment properties and the energy input from stars.

The best tracers of hot gas in the cosmic web and periphery of groups and clusters are the resonance lines of O VII and O VIII, with the O VII Heα line the strongest. Absorption from these lines (Fig. 2) has also been detected in halo gas surrounding the Milky Way[12,13,14,15], along with absorption by lower ionization lines (H I through O VI[16,17]). In the Milky Way, the hotter volume-filling ISM contains the O VII- and O VIII-bearing gas at ~2 x 10^6 K. This hot gas is thought to interact with cooler gas, producing O VI and other ions at the interface[17]. Absorption from O VI is detected around many other galaxies and in groups of galaxies[18,19], and is likewise interpreted as arising in gas clouds mixing with a hotter IGM that lies at the virial temperature of the system (~3 x 10^6 K). Based on scaling from the Milky Way observations and simulations, the hotter gas will be easily detectable with *Arcus*.

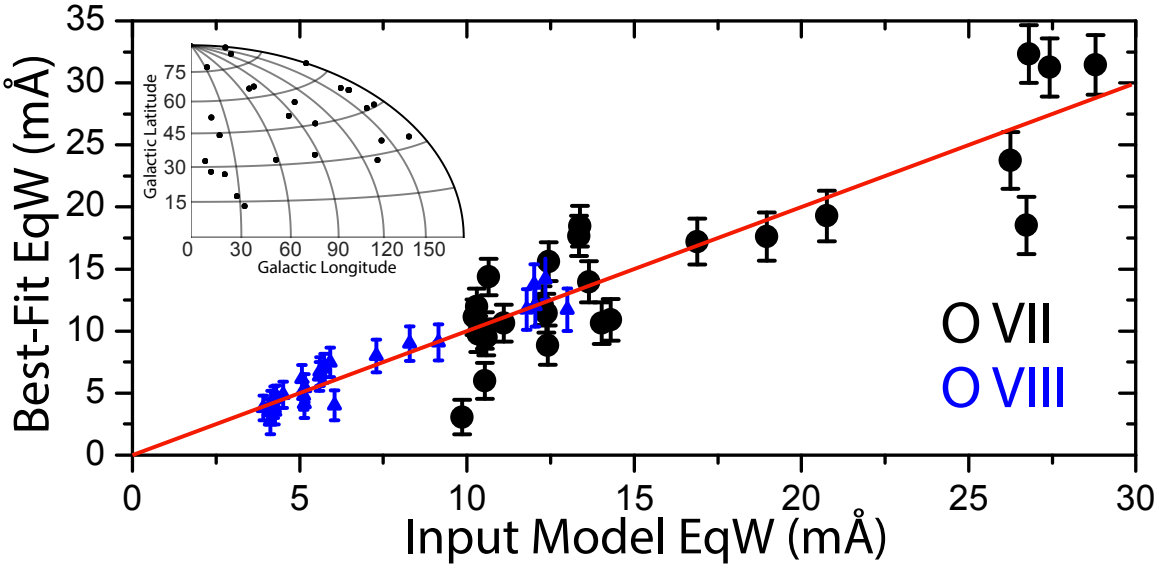

Figure 2. *Arcus* will measure the temperature distribution in the Milky Way halo using the baseline observing program (§4); this simulation of one possible model[29] shows how accurately absorption line strengths from this gas will be constrained.

Observing Strategy: Understanding feedback processes requires measurements of the mass fraction, temperature, dynamics, and volume of the hot gas. *Arcus* can detect a significant X-ray absorption line in the spectrum of distant AGN with a column of >3 x10^{19} cm^{-2} for an IGM metallicity of 20% of solar. The *Arcus* bandpass contains absorption lines from ions of C, N, O, Ne, Si, and Fe. These ions trace gas from 3 x10^5 to 10^7 K, the virial temperatures for gas associated with galaxies, groups, small clusters, and cosmic filaments.

Comparing models to data requires knowledge of the distribution of column densities (dN/dz), and simulations show that a robust determination of dN/dz is obtained with a sample of ~40 absorption systems. This is achievable with *Arcus*'s sensitivity of 4 mÅ equivalent width (EqW) and a total redshift path length of Σz_i=8, which can be obtained by observing ~20 bright, background AGN. About 10-15 of the O VII Heα detections will also yield detectable O VIII Lyα lines, with the ratio of the two providing an accurate temperature for the gas[4].

Targets were selected based on their 0.5-2 keV flux, and their number of predicted O VII absorption systems[4] detected per unit time to a fixed S/N was calculated. This figure of merit is roughly proportional to the product of the redshift and the X-ray flux, although a full simulation was done. About half of our targets are projected within 300 kpc of a luminous galaxy, about 11% are projected within twice the virial radius of a known foreground galaxy group or cluster (usually at $z < 0.2$), and at least 25% of the AGN are in a group or poor cluster of galaxies. A blind search will thus naturally sample the systems predicted to show the strongest absorption signatures.

This strategy's effectiveness is improved by monitoring AGN and performing deep observations when they become brighter than average. The *Arcus* sample's brightness variation (1σ) is ~35%, so objects >1σ above the mean can easily be selected without affecting scheduling. This either reduces the observation time per object or enables higher S/N, increasing the predicted number of absorbers. If available, all-sky X-ray data from *MAXI* or *Swift* will reveal brighter objects. However, the correlation between optical and X-ray emission is tight[20,21], so optical monitoring is also effective.

To determine the nature of each absorption site – e.g., galaxy, group, cluster – optical telescopes at the disposal of the team will obtain deep images and spectra of features detected along targeted lines of sight.

1.2 The Hot Halos of Galaxies

The missing baryon problem applies on galactic scales as well as cluster scales. In a spiral galaxy with a stellar luminosity equal to that of the Milky Way, only 1/4 of the expected baryons are manifest. This discrepancy becomes worse with decreasing galaxy mass. The resolution must be that the gas surrounds the galaxy either as a bound hot halo or as a larger halo with mass extending beyond the virial radius (R_{200}). In the standard galaxy formation process paradigm[22], accretion of gas onto massive galaxies proceeds through a combination of low-entropy "cold flows" and gas that is shocked at large radii (near the virial radius), reaching temperatures characteristic of the gravitational potential well, typically ~few x 10^6 K. The gas is denser close to the galaxy, so there is a radius (~50 kpc) within which the cooling time is less than a Hubble time. The gas within this radius can cool and accrete onto the galaxy, supplying fresh material that can form a cold disk that, in turn, is converted into stars. However, almost all of the hot halo mass lies beyond 50 kpc (Fig. 3).

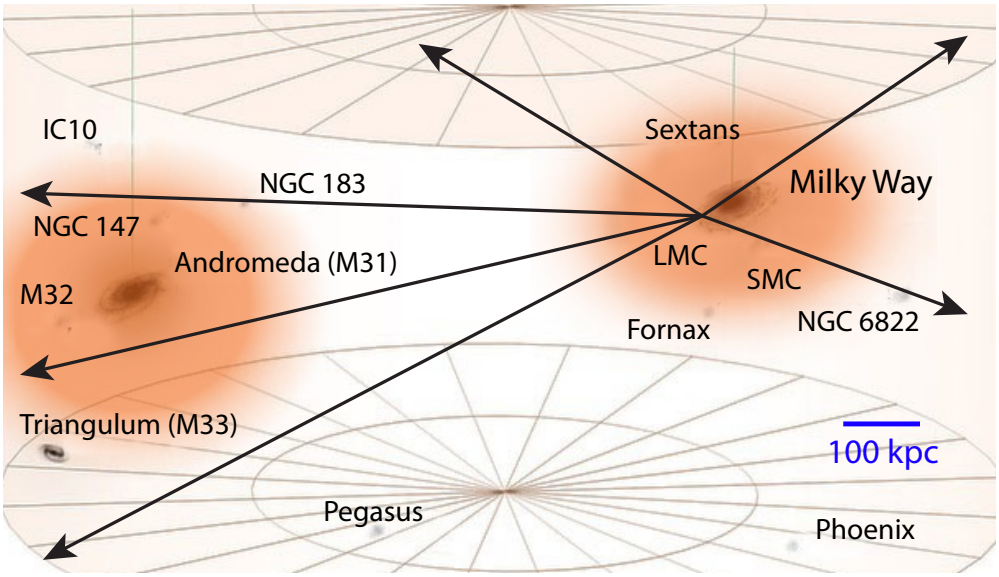

Figure 3. Every extragalactic sight line probes the Milky Way (MW) hot halo, allowing measurements of the density, temperature, mass distribution, and velocity of the gas therein, while multiple lines probe nearby galaxies like M31.

Analogous to the study of the WHIM on larger scales, the mass and extent of the Milky Way's hot gaseous halo depends on the effectiveness of stellar feedback, past heating from an AGN, and whether heating from an early population of stars occurred during the nascent stages of galaxy formation. Detailed simulations[23] that account for these processes predict the spatial distribution of the metals and the density and dynamics of the hot gas, properties uniquely testable using *Arcus*.

Observational studies have shown[15] an extensive halo around the Milky Way (in emission and absorption) and around isolated external galaxies (in emission). For both targeted observations and stacking analyses of external galaxies, X-ray emission is detected to about 50 kpc, and the enclosed mass in the hot gas within 50 kpc is typically ~5 x 10^9 M_{sun} for galaxies with optical luminosities above that of the Milky Way (L*)[23,24,25,26,27]. When the radial density is extrapolated from 50 kpc to R_{200} (~250 kpc), the hot halo mass accounts for 1/3 - 1/2 of the missing baryons. If this extrapolation

continues, the missing baryons would extend to 2-5 R_{200}, a region currently unexplored by any observatory and uniquely probed by *Arcus*.

O VII absorption by external galaxies traces hot galactic halo gas, but it has yet to be detected either for individual spectra, or in stacked *Chandra* spectra[28], in which there were too few galaxies with L > L* and with impact parameters less than the virial radius. Simulations predict that galaxies of the Milky Way's mass or larger will have significant hot gas halos (within 200 kpc) but lower mass galaxies will not have significant hot gas halos. By measuring the absorption as a function of both impact parameter and galaxy mass, *Arcus* can determine the masses of hot halos and the range of halo mass among galaxies, testing simulations.

Arcus will also carry out cornerstone investigations of the Milky Way's hot halo that will reveal its shape and radial extent, as well as its mass, metallicity, temperature, and dynamics (see §1.1 and Fig. 2). *Arcus*'s sensitivity will yield multiple Milky Way absorption lines from several ions, including all ionization stages of oxygen, as seen through the ISM along the line of sight toward every background AGN.

Hot gas in the Milky Way's halo can also have different velocity structures resulting from the galaxy's formation and current activity. The gas in the extended hot Milky Way halo (best traced with O VII and O VIII absorption) may have low angular momentum, or it may be nearly co-rotating, depending on how our galaxy formed. With *Arcus*, a co-rotating halo is easily distinguished from a non-rotating halo by the velocity centroid of the O VIII absorption line observed along different lines of sight (Fig. 4). These absorption spectra will detect or place limits on whether the halo gas is inflowing or outflowing, which produces a global blueshift or redshift, respectively. Global flows are most evident at high latitudes, while rotation effects are strongest at low latitudes, so the two phenomena can easily be separated.

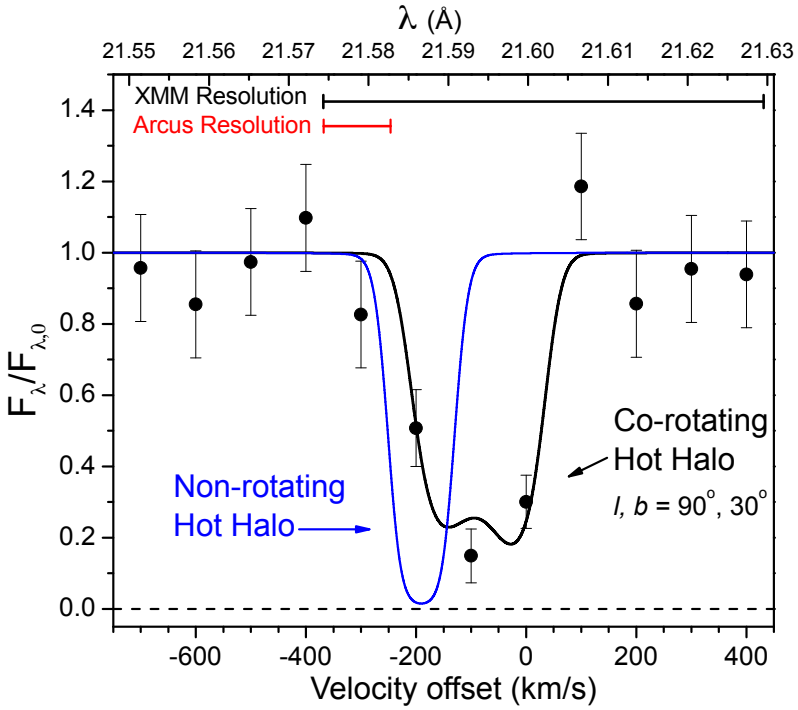

Figure 4. Galaxy formation produces either a non-rotating halo or a nearly co-rotating halo. *Arcus* can distinguish between the two models by the difference in line centroids. For the co-rotating halo, the line shape reveals the radial extent and angular momentum of the hot gas.

1.3 Dust Composition in the Milky Way

The galaxy's hot halo origin and evolution are also connected to processes occurring in the disk of the Milky Way. X-ray spectra provide independent measures of elemental abundances and dust properties that are largely unaffected by depletion onto dust grains, measuring the composition of the dust by resolving the molecule-specific fine structures near

the absorption edges and comparing them to laboratory-measured spectra of dust analogs. Further, abundance measurements from *Chandra* and *XMM-Newton*, determined through measurements of the edge depths, have ~10% uncertainties for oxygen and neon for a handful of sight lines[29,30] but are higher (often >20%) for other elements such as magnesium and iron[30,31,32,33,34,35]. *Arcus* will easily be able to determine these abundances with values of hydrogen column density derived from other wavelength regimes[36] and cross-checked against the broadband absorption found with *XMM-Newton* and *Chandra* data, where available. These data will provide much-needed constraints on dust grain models, which are crucial in many areas of study.

In particular, the foreground dust emission in cosmic microwave background (CMB) polarization measurements[37] is sensitive to grain composition. The common way of accounting for polarized emission from foreground dust is to scale the observed emission at a certain frequency from microwave missions like *WMAP* or *Planck* to the frequency that the CMB polarimeter is sensitive to, usually by assuming a constant emissivity value and temperature. However, recent work has shown that the expected polarized dust emission is highly dependent on grain composition. If there are magnetic inclusions in the silicate, the degree of linear polarization increases by a factor of ~4 from 100 GHz to 300 GHz, with the exact changes depending on what type of magnetic inclusion is in the dust, such as Fe_2O_3, Fe_3O_4, or metallic Fe[78,79]. Spectroscopy from *Arcus* will allow us to clearly distinguish between these dust types, and thus determine the expected foreground linear polarization. Further, because dust is ubiquitous throughout the Galaxy, almost every observation made with *Arcus* will contain dust features, giving us an unmatched data set with which to determine elemental abundances and grain compositions. Based on the *XMM-Newton* Serendipitous Survey Catalog, ~1000 sources, mainly bright X-ray binaries (XRBs), have fluxes > 5×10^{-12} erg cm^{-2} s^{-1} in the *Arcus* bandpass, making them targets for which both the source and intervening ISM can easily be observed. A 100 ks exposure will detect absorption lines > 3.5 mÅ EqW (3σ). The oxygen abundance will be measurable to <10% for almost all sightlines; similar data for neon and iron will be measurable along any of over 400 sightlines. Neither *Chandra* nor *XMM-Newton* can approach what *Arcus* will provide (Fig. 5), either in terms of quality of spectra or quantity of sightlines.

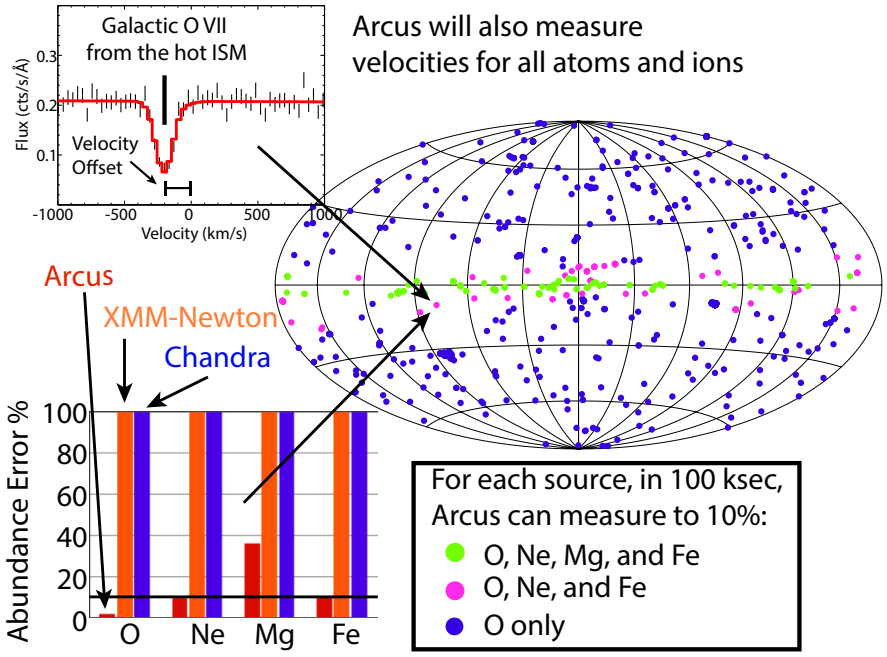

Figure 5. *Arcus* will map velocities and abundances for all phases of the Milky Way ISM with accuracies and precisions impossible to achieve with current observatories.

Observing Strategy: The O VII and O VIII ions are the best probes of the temperature of the hot halo in a galaxy, as they are both present at the virial temperatures of the Milky Way and external galaxy halos and will be measured along all sightlines with *Arcus*. Measuring the distribution of these two ions reveals the temperature distribution with radius and

the dynamical gas properties along individual sight lines, yielding greatly improved determinations for the halo gas mass and metallicity[46] (Fig. 2).

The O VII Heα and Heβ line ratios in the Milky Way will return the opacity of the absorbing gas, while the ratios of O VII to O VIII yield temperatures. The average EqWs of O VII Heα and O VIII Lyα are 20 mÅ and 10 mÅ, respectively[15], and the anticipated values of O VII Heβ and O VIII Lyβ are 7 mÅ and 3.5 mÅ, at or above *Arcus*'s sensitivity limit.

Simulations were performed to determine how the number of sight lines affects the constraints on the Milky Way density distribution. This program uses the sightlines from the LSS program (above) plus five additional targets in directions across the Milky Way. Using this sample, the density normalization and power-law density slope can be measured to accuracies of ±8% and ±5%, respectively.

For the Milky Way hot halo, the metallicity vs. radius will be determined. The radial distribution of O VII and O VIII emissivities, $n_o/n_e(r)$, is known from *XMM-Newton* studies[29], so by using *Arcus* data to obtain an accurate determination of the spatial absorption line distribution, $n_o(r)$, the electron and the metallicity distributions, $n_o/n_e(r)$, can be derived.

The absorption line spectra will easily distinguish between a stationary and rotating hot halo of gas (Fig. 4), another fundamental property for which theoretical models differ. Inflows or outflows with mean velocities >30 km s^{-1} will also be detectable (most evident in high Galactic latitude lines of sight).

Arcus can also measure properties of Messier 31 and other nearby galaxies. The absorption properties of external galaxies were estimated using Milky Way models[15,37] projected onto the sky around each galaxy. Assuming constant metallicity with radius, an equivalent width exceeding 3.5 mÅ in O VII is detectable in the spectra of background AGN whose line of sight is within 320 kpc (1.3 R_{200}) and the O VIII line is detectable within 140 kpc (0.6 R_{200}). With the targets selected for the LSS program, about 24 O VII absorption systems will be due to luminous nearby galaxies, allowing radial O VII and O VIII distributions to be mapped.

M31 has 6 bright AGN projected at galactic radii of 100-200 kpc, permitting absorption to be mapped with galactic radius in unprecedented detail (Fig. 3). With v_{Helio} = -300 km s^{-1}, it is separated in velocity from the Milky Way's local plasmas by 19 mÅ at O VIII, easily resolvable by *Arcus*. Two targets are in the direction of M33, so we should gain information on that galaxy as well.

For Milky Way disk absorption, sightlines to 56 sources were selected because they are bright, cover a range of densities and thus ISM environments ($N_H \sim 10^{21}$–10^{22} cm^{-2}), and have IR and/or optical data, allowing multiwavelength examinations of the ISM towards each.

2. BLACK HOLE FEEDBACK

2.1 Wind Outflows from AGN

Understanding how supermassive black holes formed and evolved with their host galaxies, shaping the Universe over cosmic time, involves closely examining their inner regions. This area is thought to be the launching location for outflows of matter and energy from the black hole via winds and jets. Depending on the mass, energy and momentum involved, these outflows may have a major role in galaxy formation and evolution via the feedback they provide[38,39,40].

The large-scale, downstream effects of black hole feedback will be examined through observations of dust and cool gas motions by longer-wavelength missions such as *Herschel*, *ALMA* and *JWST*. *Arcus* offers a unique window on these flows close to their launching point, providing critical insights into AGN structure and energetics. Comparing flow properties at the launch point and downstream is the only means to fully understand how such feedback acts on the host galaxy environment. AGN spectra are most complex at soft X-ray energies, where emission and absorption by dozens of ions in photoionized gas are all superimposed on the spectrum. Disentangling these features, which are strongly time-dependent, requires both high spectral resolution and effective area, but will reveal the velocity distribution, chemical composition, ionization states, locations, and overall structure of the gas intrinsic to AGN (Fig. 6).

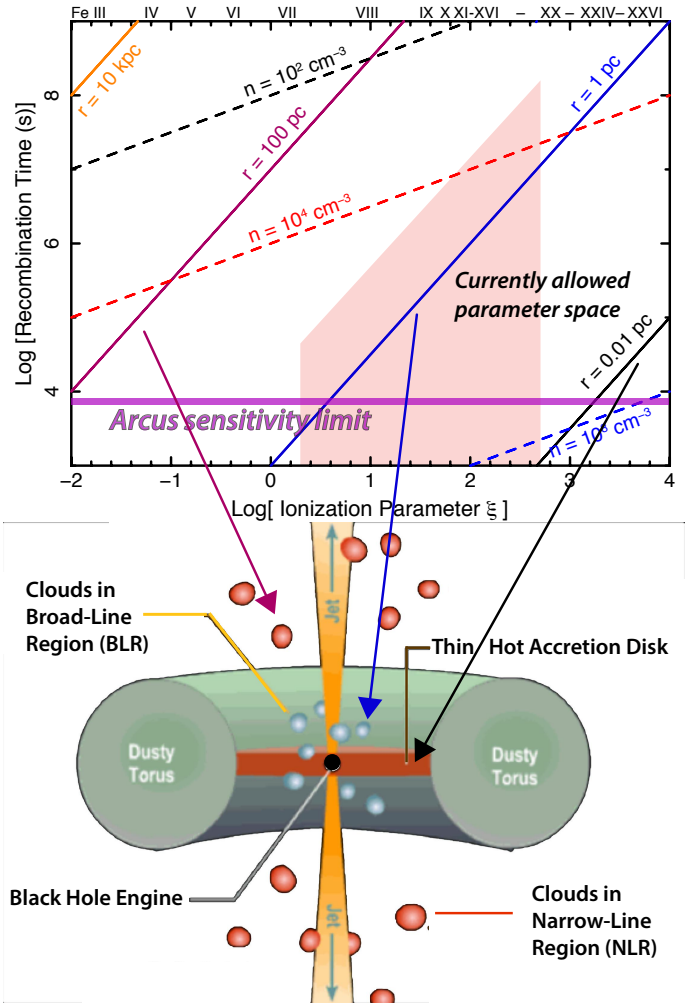

Figure 6. *Top*: Recombination time scale for iron ions as a function of ionization parameter for the ionizing spectral energy distribution of NGC 5548. The y-axis corresponds to the time range that *Arcus* will sample. Solid lines indicate distance from the black hole, dashed lines hydrogen density. Roman numerals above the plot indicate the ionization parameters where the various iron ions have their peak concentration. *Bottom*: Model of an AGN showing distances of the physical structures corresponding to the distances *Arcus* can probe.

UV observations can resolve small column density outflow velocities to a few tens of km s^{-1}, but the UV only measures gas in lower states of ionization. The bulk of the outflow in AGN winds is much more highly ionized and only detectable in X-rays[41,42]. As shown in Fig. 7, the spectral resolution of existing X-ray grating spectrometers (several hundred km s^{-1}) and their low effective areas allow measurements for only a few of the brightest AGN with *XMM-Newton* or *Chandra* using exposure times of >300 ks (e.g., NGC 3783[43]; Mrk 509[44]; NGC 5548[45]). *Athena* will not improve this situation significantly.

Arcus will be able to characterize the two-dimensional ionization-velocity plane and deduce the structure, density and location of all physical and kinematic components of the outflow. *Arcus* will measure an average of 90 absorption lines per AGN, including K-shell C, N, O and Ne as well as L-shell Fe. The mission is ideally suited to the detection of density-sensitive Fe XX, XXI, and XXII lines which reveal the wind launching radius, mass outflow rate, and kinetic power. These measurements can then be compared to the net accretion rate as derived from the observed continuum properties of the AGN to understand how the mass outflow and inflow rates compare. These data will constrain or reveal the launching mechanism(s) of the wind (e.g., magnetic, radiative, or thermal pressure[47]).

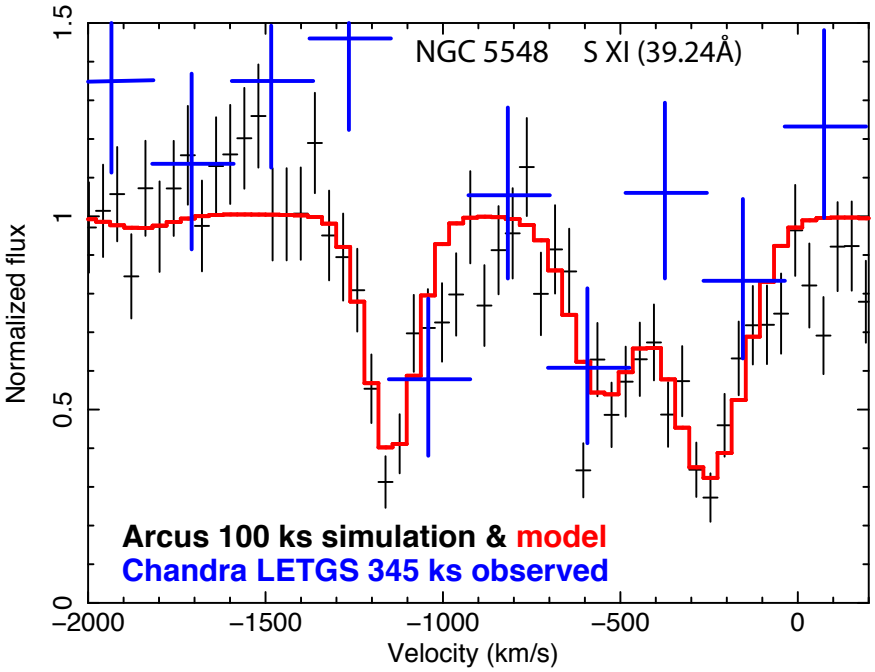

Figure 7. *Arcus* will resolve features in SMBH outflows comparable to those seen in optical/UV bands, a capability that existing X-ray spectrometers cannot match regardless of exposure time.

Because very long (>300 ks) exposure times with *XMM-Newton* or *Chandra* are required for the brightest AGN, only a few have accurately measured chemical compositions[46]. *Arcus* can obtain abundances in a much larger sample of dimmer sources and for many more elements in the brighter sources. These measurements will facilitate detailed study of the conditions for star formation close to the galactic core, including the chemical composition of the outflows reaching large distances from the AGN.

2.2 Outflows from X-ray Binary Systems

XRBs function as nearby laboratories in which to explore the predictions of General Relativity. They also serve as microcosms of larger AGN, probing the nature of the disk winds and jets that drive feedback in more massive systems. *Arcus* will easily detect an average of 30 absorption lines per XRB system, including density-sensitive Fe XX, XXI, and XXII lines in outflows from Galactic Black Holes (GBHs), making it possible to determine wind launching radii, mass outflow rates, and driving mechanisms[38,47], which have informative synergies with outflows and feedback in AGN. *Arcus* can detect these lines far more efficiently than any current, approved or planned observatory. Wind evolution studies on the dynamical timescale of the outflow will be possible, revolutionizing our understanding of disk-wind interactions.

Arcus can also easily detect and monitor relativistic oxygen and iron emission lines from accretion disks around neutron stars and stellar-mass black holes[47,48]. Modeling these line profiles can place important limits on neutron star radii, and can even probe the ultra-dense matter equation of state. In this way, *Arcus* can provide an independent perspective on *NICER* core science goals.

Observing Strategy: Because stacked spectra of these AGN reveal only the time-averaged state of these sources, repeated deep observations at different time intervals are needed to measure the response of the outflow to continuum variations, thereby determining the density and distance of the outflow. *Arcus* will observe ~10 bright, nearby AGN with prominent outflows, using total exposure times of 100-300 ks with cadences ranging from days to months. Additionally, *Arcus* will observe ~100 AGN identified through the *ROSAT* all-sky survey with shallower exposures to allow for absorption line detections. *Arcus's* high spectral resolution will resolve velocity components to the ~100 km s^{-1} level, sufficient to disentangle and study the physics of each velocity component. The ionization parameter space is

sampled using the K-shell transitions of all ions from elements like C, N, O, and Ne as well as L-shell transitions of Fe. These ions cover several decades in ionization parameter. Absorption features from Rydberg series transitions up to n=6 are easily measured for abundant elements, constraining the geometry and dynamics further. Lines from rare elements will be detected in the stacked spectra, allowing their abundances to be measured. The observing strategy for XRBs will be similar, focusing on the 10 brightest systems with strong outflows for the core science and following these up by examining the 56 additional lines of sight toward bright XRBs utilized in the LSS observing strategy.

3. STELLAR SYSTEMS

The wealth of emission lines in the X-ray spectrum yields detailed measurements of electron temperatures and densities in the magnetically heated and/or shocked plasmas found in the outer atmospheres of normal stars. *Arcus* will make critical contributions to two main areas of stellar science: 1) high energy processes in young stars and their effects on protoplanetary disks, and 2) stellar coronal heating.

3.1 Young stars and planets

Young stars show high levels of magnetic activity relative to their main sequence counterparts[49], either because the stellar dynamo is intrinsically more active in youth, or because magnetically-controlled accretion drives a response in the magnetic upper atmosphere. Differentiating between these hypotheses requires high resolution X-ray spectroscopy to explore the accretion-driven physics.

Only a dozen young stars have been observed using the *Chandra* and *XMM-Newton* gratings. The observations confirm the basic accretion shock model: Ne IX and O VII lines indicate high densities at relatively low temperatures compared with pure stellar coronae[50,51]. The standard paradigm posits a gentle slowing and cooling of the post-shock plasma when the shocked gas hits the stellar corona, but a variety of data[52,53] suggests a more turbulent interaction between the accretion stream and the stellar atmosphere (Fig. 8).

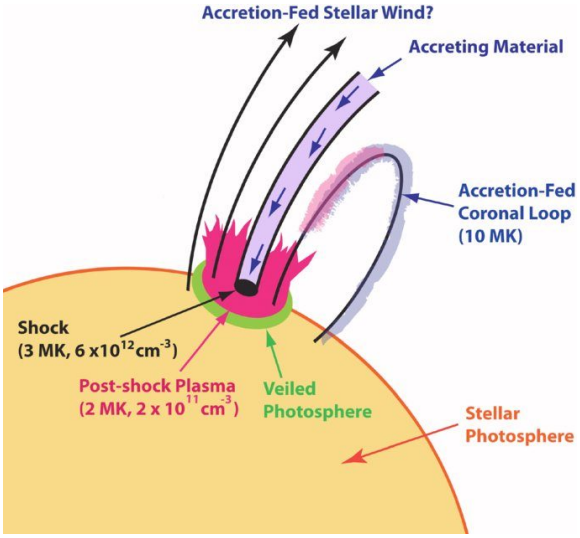

Figure 8. Illustration of the accretion shock impacting onto a young star. *Arcus* will be able to detect potential turbulent broadening of the O VII line in the post-shock plasma. Figure from Brickhouse et al (2010)[58], © AAS. Reproduced with permission.

Arcus measurements of the shocked atmosphere will address several open questions in star and planet formation. For example, observations of accreting young stars show that they are spinning slower than expected, given that they are adding mass and contracting. Accretion-driven stellar winds, seen via *Arcus* absorption line measurements in the post-shock gas and critical for understanding star and planetary disk formation[54], may be the answer to this conundrum.

The effects of the star on its disk are also not well understood; we do not yet know how rapidly the high-energy radiation of young stars disperses their gas disks, ending the phase of major planet formation. The stellar magnetic field and high-energy radiation not only ionize the disk and drive the magnetorotational instability (MRI), enabling accretion, but they also drive gas motions in the radial direction to catalyze planet formation. X-rays from the star[55] can quickly photoevaporate the gas in the disk (~10 Myr), setting the timeframe for planet growth.

Thousands of nearby planets orbiting other stars have been discovered via optical and IR spectra and photometric data. These include previously unknown and unexpected types, such as the "Hot Jupiters." X-ray studies have a key role to play in understanding the thermal profiles and atmospheric chemistry of these objects. The upper atmosphere and exosphere of one such exoplanet, HD 189733b, have been detected with *Chandra*. The transit depth and width in X-rays were found to be deeper and wider than optical, IR or UV transits[56].

While low-altitude physics of exoplanet atmospheres is accessible through IR observations, *Arcus* will be the first mission able to directly measure the density and infer the composition of the high-altitude outer layers of exoplanet atmospheres. A typical target will be a moderately X-ray bright host star ($F_X \sim 10^{-12}$ erg cm^{-2} s^{-1}) orbited by an exoplanet with an optical transit depth of 3%; this system will display an X-ray transit depth of ~12% (Fig. 9). Observing such a source for 10 transits of 30 ks each (total 300 ks), we will detect the exosphere and determine its density. A few good targets are now known, and the list will be strongly increased by *TESS*, which will launch in 2017 and conduct an all-sky survey for transiting exoplanets.

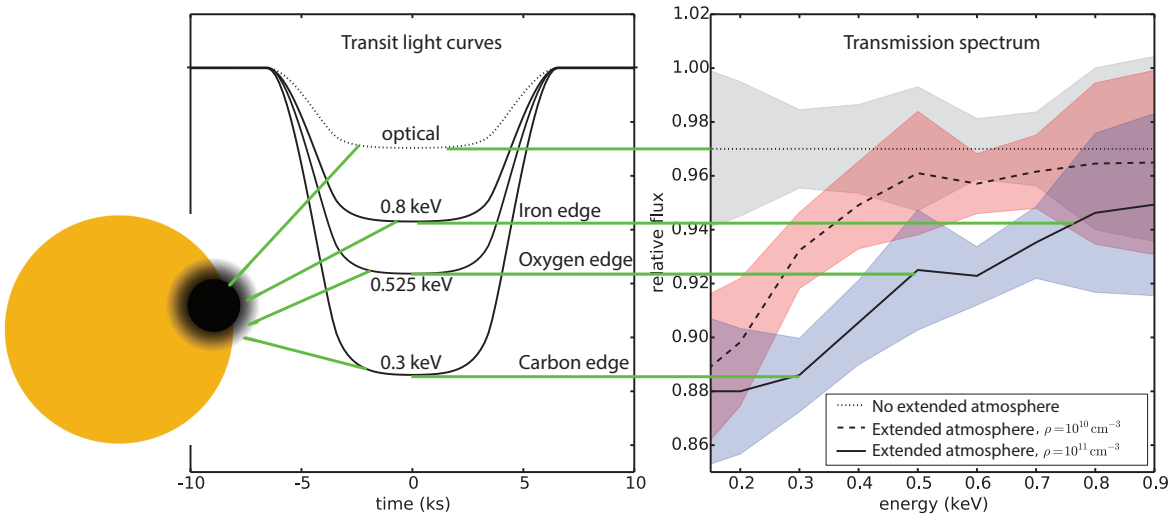

Figure 9. Exoplanets in close orbits can form extended evaporating atmospheres (to 1.7 optical radii). The density and extent of high-altitude atmospheric layers can be studied with *Arcus* through energy-resolved transit observations sensitive to different elements. Soft X-ray photons are absorbed by low column densities in the atmosphere, causing deep transit light curves, while harder X-rays probe yet deeper layers.

Observing Strategy: *Arcus* uniquely enables the detection of a set of He-like diagnostic lines from the onset of the accretion shock at 3 MK (Ne IX) through the coolest X-ray emitting component at 1 MK (C V). The four diagnostic lines from each He-like ion will map density, absorbing column and turbulence as functions of temperature[57,58]. The spectral resolving power of *Arcus* will allow tight constraints to be placed on the turbulence in the plasma using the O VII line.

In order to cover a range in rotation period, stellar type, and age as well as differences in orientation, a sample of 14 young stars will be studied, including three non-accreting young stars as a control group. Comparisons with the sample of main sequence coronal stars will also be possible. Exposure times are based on obtaining S/N=25 in the O VII resonance line in the 12 brightest targets (S/N=5 in the remaining 2), as predicted from *Chandra* and/or *XMM-Newton* observations of each source.

3.2 Coronal sources

The solar corona is heated to more than 400 times the temperature of the photosphere by a magnetic dynamo not well understood[59]. Active stars can have up to 10^5 times the coronal luminosity of the sun and have similar anomalously hot coronae. Understanding the roles of rotation and magnetic fields in stellar evolution is emphasized in the 2010 Decadal Survey[1].

One of the popular coronal heating models developed circa 1990 is the impulsive heating, or "nanoflare,"model, wherein multiple loops of magnetically-confined plasma are randomly heated by energetic particles accelerated down the loop legs[60]. Each loop heats up and ionizes quickly, then cools and recombines slowly. On average, the charge state of the gas lags the local temperature, leading to a recombination-dominated plasma.

Recently, a predictive Alfvén wave heating model has been proposed[61], in which turbulently broadened lines and a steady, isothermal plasma are predicted. Near-isothermal plasmas in some stellar coronae[62] are suggestive of this mechanism, but nanoflare models may also produce such features[63].

The weak dielectronic recombination (DR) satellite lines (reviewed in solar context[64] but also present in stellar coronae) are highly sensitive to recombining conditions, becoming stronger at lower temperatures[65]. The accumulated *Chandra* spectrum of Capella shows evidence for these features (Fig. 10), but lacks the resolution necessary to measure them accurately. *Arcus* will allow these to be used as diagnostics to test coronal heating models for a range of stellar types.

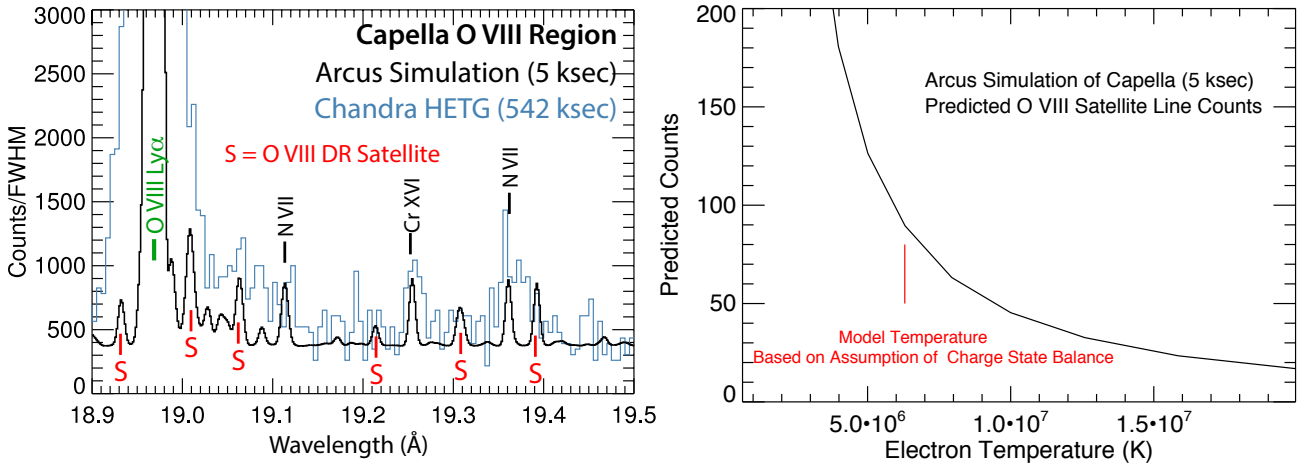

Figure 10. *Left*: Simulated *Arcus* O VIII region of Capella overlaid on the *Chandra*/HETG spectrum. DR satellite lines of O VIII marked (S) are identified using the AtomDB v3.0 spectral database. *Right*: Predicted *Arcus* counts in the six labeled satellite lines as a function of electron temperature for Capella, scaled from the O VIII Lyα flux. The collisional ionization equilibrium model is dominated by 6.3 MK plasma, where the DR count rate is very sensitive to electron temperature; with 100 counts, this temperature can be measured to ±0.5 MK, revealing if the plasma is in equilibrium or not.

Observing Strategy: *Arcus* spectra will allow the distribution of electron temperatures in the coronal loops to be determined[66] and test the assumption that the plasma is in ionization equilibrium. With both higher effective area and spectral resolution than the *Chandra* gratings, *Arcus* will enable detection of several individual DR lines from highly charged ions (Fig. 10). The temperature sensitivity of the strong lines derives primarily from the charge state distribution and assumes ionization equilibrium. The emission measure distribution (EMD)[67], using strong lines from many ions, can be reliably reconstructed using this assumption. Using the EMD, we will then predict the properties of the weak DR lines. If the plasma is not in equilibrium but is instead recombining, the DR lines will be stronger than predicted and will signal the degree of non-equilibrium. *Arcus* will observe 22 stellar coronal sources, including single and binary systems, and covering a range of stellar types, magnetic activity levels, and rotations, including the rapidly rotating prototype AB Dor. These observations will enable measurement of the line ratio temperature diagnostic to 5σ using the six DR satellite lines of O VIII marked in Fig. 10 for Capella. Lines from other ions, including satellites, will ensure self-consistent analysis.

4. OBSERVATORY SCIENCE

Arcus will address a large range of additional scientific questions once the baseline mission is completed. More exoplanet transits, as well as white dwarf binary systems including cataclysmic variables and super-soft sources that may be the progenitors of Type Ia supernovae could be observed, and some extended source observations should be possible. Other possibilities include exploring X-ray faint stars such as M dwarfs that fall below the *Chandra* or *XMM-Newton* grating detection threshold. Two possible observations are discussed below.

4.1 Stellar Winds

Stellar mass loss enriches and energizes the ISM while altering the evolution of the star. However, measured mass loss rates are uncertain by up to an order of magnitude, and systematically differ from theoretical predictions[68,69]. Constraining these rates to within a factor of two is key to testing hot-star evolution models[70]. The emission line profiles of stellar winds are sensitive to their density, ionization, geometry, kinematics and any inhomogeneities in the flow[71,72]. High-resolution spectra from *Chandra* and *XMM-Newton* have enabled progress but possess limited sensitivity; resolving powers of 1500-2000 and larger A_{eff} are needed[73,74]. *Arcus* will fully resolve several emission lines in stars such as ζPupis with terminal velocities of ~2000 km s^{-1}. For B-stars with winds as slow as ~800 km s^{-1}, line shifts and asymmetries may reveal discrete features from small structures in a currently unexplored, but theoretically possible regime.

4.2 SN1987A

SN1987A has transitioned into a young SNR with a complex soft X-ray spectrum. X-ray spectra already show broad and shifted lines from a non-equilibrium plasma. Accurate and precise measurements of the abundances would constrain models of the progenitor SN[75,76] and allow us to confirm suggestions that dust destruction is ongoing[77]. *Arcus* has both the resolution and sensitivity to allow accurate modeling of the shocked plasma spectrum and thus make robust abundance measurements.

REFERENCES

[1] National Research Council, "New Worlds, New Horizons in Astronomy & Astrophysics," http://www.nap.edu/catalog/12951/New-Worlds-New-Horizons-In-Astronomy-and-Astrophysics (2010).

[2] Kouveliotou, C. et al., "Enduring Quests, Daring Visions (NASA Astrophysics in the Next Three Decades)," eprint arxiv:1401.3741 (2014).

[3] Smith, B.D. et al., "The Nature of The Warm/Hot Intergalactic Medium. I. Numerical Methods, Convergence, and O VI absorption," The Astrophysical Journal, 731, 6 (2011).

[4] Cen, R., "Coincidences Between O VI and O VII Lines: Insights from High-Resolution Simulations of the Warm-Hot Intergalactic Medium," The Astrophysical Journal, 753, 17 (2012).

[5] Marinacci, F. et al., "Diffuse Gas Properties and Stellar Metallicities in Cosmological Simulations of Disc Galaxy Formation," Monthly Notices of the Royal Astronomical Society, 442, 3745-3760 (2014).

[6] Schaye, J. et al., "The Eagle Project: Simulating the Evolution and Assembly of Galaxies and their Environments," eprint arxiv:1407.7040 (2014).

[7] *Planck* Collaboration, "*Planck* Intermediate Results," Astronomy & Astrophysics, 557, A52 (2013).

[8] Kravtsov, A.V. & Borgani, S., "Formation of Galaxy Clusters," Annual Review of Astronomy & Astrophysics, 50, 353-409 (2012).

[9] Eckert, D. et al., "The Gas Distribution in the Outer Regions of Galaxy Clusters," Astronomy & Astrophysics, 541, A57 (2012).

[10] Simionescu, A. et al., "Thermodynamics of the Coma Cluster Outskirts," The Astrophysical Journal, 775, 4 (2013).

[11] Reiprich, T.H. et al., "Outskirts of Galaxy Clusters," Space Science Reviews, 177, 195-245 (2013).

[12] Nicastro, F. et al., "*Chandra* Discovery of a Tree in the X-ray Forest Toward PKS 2155−304: the Local Filament?," The Astrophysical Journal, 573, 157-167 (2002).

[13] Rasmussen, A., Kahn, S.M., & Paerels, F., "X-ray IGM In The Local Group," in the IGM/Galaxy Connection: the Distribution of Baryons At z=0," 281, 109 (2003).

[14] Wang, Q.D. et al., "Warm-Hot Gas in and around The Milky Way: Detection and Implications of O VII Absorption Toward LMC X-3," The Astrophysical Journal, 635, 386-395 (2005).

[15] Miller, M.J. & Bregman, J.N., "The Structure of The Milky Way's Hot Gas Halo," The Astrophysical Journal, 770, 118 (2013).

[16] Fox, A.J. et al., "Multiphase High-Velocity Clouds Toward HE 0226−4110 and PG 0953+414," The Astrophysical Journal, 630, 332-354 (2005).

[17] Wakker, B.P. et al., "Characterizing Transition Temperature Gas in the Galactic Corona," The Astrophysical Journal, 749, 157 (2012).

[18] Werk, J.K. et al., "The COS-HALOS Survey: an Empirical Description of Metal-Line absorption in the Low-Redshift Circumgalactic Medium," The Astrophysical Journal Supplement Series, 204, 17 (2013).

[19] Stocke, J.T. et al., "Absorption-Line Detections of 10^5 -10^6 K Gas in Spiral-Rich Groups of Galaxies," The Astrophysical Journal, 791, 128 (2014).

[20] Jorstad, S.G. et al., "Flaring Behavior of The Quasar 3C454.3 across the Electromagnetic Spectrum," The Astrophysical Journal, 715, 362-384 (2010).

[21] Cameron, D.T. et al., "Correlated X-ray/Ultraviolet/Optical Variability in the Very Low Mass AGN NGC 4395," Monthly Notices of the Royal Astronomical Society, 422, 902-912 (2012).

[22] Mo, H., Van Den Bosch, F.C., & White, S., [Galaxy Formation and Evolution], Cambridge University Press, Cambridge, UK (2010).

[23] Cen, R. & Fang, T., "Where Are The Baryons? III. Nonequilibrium Effects and Observables," The Astrophysical Journal, 650(2), 573-591 (2006).

[24] Anderson, M.E. & Bregman, J.N., "Detection of a Hot Gaseous Halo Around the Giant Spiral Galaxy NGC 1961," The Astrophysical Journal, 737, 22 (2011).

[25] Dai, X. et al., "*XMM-Newton* Detects A Hot Gaseous Halo in the Fastest Rotating Spiral Galaxy UGC 12591," The Astrophysical Journal, 755, 107 (2012).

[26] Humphrey, P.J. et al., "The ELIXR Galaxy Survey. II. Baryons and Dark Matter in an Isolated Elliptical Galaxy," The Astrophysical Journal, 755, 166 (2012).

[27] Bogdán, Á. et al., "Detection of a Luminous Hot X-ray Corona around the Massive Spiral Galaxy NGC 266," The Astrophysical Journal, 772, 98 (2013).

[28] Anderson, M.E. & Bregman, J.N., "Modeling X-ray Emission around Galaxies," The Astrophysical Journal, 785, 67 (2014).

[29] Miller, M.J. & Bregman, J.N., "Constraining the Milky Way's Hot Gas Halo with O VII and O VIII Emission Lines," The Astrophysical Journal, 800, 14 (2015).

[30] Costantini, E. et al., "*XMM-Newton* Observation of 4U 1820-30," Astronomy & Astrophysics, 539, A32 (2012).

[31] Pinto, C. et al., "Interstellar Medium Composition Through X-ray Spectroscopy of Low-Mass X-ray Binaries," Astronomy & Astrophysics, 551, A25 (2013).

[32] Paerels, F. et al., "Interstellar X-ray Absorption Spectroscopy of Oxygen, Neon, and Iron with the *Chandra* LETGS Spectrum of X0614+091," The Astrophysical Journal, 546, 338-344 (2001).

[33] Takei, Y. et al., "O and Ne K absorption Edge Structures and Interstellar Abundance Toward Cygnus X-2," The Astrophysical Journal, 581, 307-314 (2002).

[34] Ueda, Y. et al., "Study of The Galactic Interstellar Medium from High-Resolution X-Ray Spectroscopy: X-Ray Absorption Fine Structure and Abundances of O, Mg, Si, S, and Fe," The Astrophysical Journal, 620, 274-286 (2005).

[35] Juett, A.M. et al., "High-Resolution X-Ray Spectroscopy of the Interstellar Medium. II. Neon and Iron Absorption Edges," The Astrophysical Journal, 648, 1066-1078 (2006).

[36] Kalberla, P.M.W. et al., “The Leiden/Argentine/Bonn (Lab) Survey of Galactic HI,” Astronomy & Astrophysics, 440(2), 775-782 (2005).

[37] Barkats, D. et al., “Degree-Scale Cosmic Microwave Background Polarization Measurements from Three Years of BICEP1 Data,” The Astrophysical Journal, 783, 67 (2014).

[38] Miller, J.M. et al., “*Chandra* Spectroscopy of MAXI J1305–704: Detection of an Infalling Black Hole Disk Wind?,” The Astrophysical Journal, 788, 53 (2014).

[39] Silk, J. & Rees, M.J., “Quasars and Galaxy Formation,” Astronomy & Astrophysics, 331L, 1 (1998).

[40] Furlanetto, S.R. & Loeb, A., “Intergalactic Magnetic Fields from Quasar Outflows,” The Astrophysical Journal, 556, 619-634 (2001).

[41] Arav, N. et al., “Multiwavelength Campaign on Mrk 509 X. Lower Limit on the Distance of the Absorber from HST COS and STIS Spectroscopy,” Astronomy & Astrophysics, 544, A33 (2012).

[42] Behar, E., “Density Profiles in Seyfert Outflows,” The Astrophysical Journal, 703, 1346-1351 (2009).

[43] Kaspi, S. et al., “The Ionized Gas and Nuclear Environment in NGC 3783. I. Time‐Averaged 900 Kilosecond *Chandra* Grating Spectroscopy,” The Astrophysical Journal, 574, 643-662 (2002).

[44] Kaastra, J.S. et al., “Multiwavelength Campaign on Mrk 509 VIII. Location of the X-ray Absorber,” Astronomy & Astrophysics, 539, A117 (2012).

[45] Kaastra, J.S. et al., “A Fast and Long-Lived Outflow from the Supermassive Black Hole in NGC 5548.,” Science, 345, 64 (2014).

[46] Steenbrugge, K.C. et al., “Multiwavelength Campaign on Mrk 509 VII. Relative Abundances of the Warm Absorber,” Astronomy & Astrophysics, 534, A42 (2011).

[47] Miller, J.M. et al., “The Magnetic Nature of Disk Accretion onto Black Holes.,” Nature, 441, 953 (2006).

[48] Madej, O.K. et al., “X-ray Reflection in Oxygen-Rich Accretion Discs of Ultracompact X-ray Binaries,” Monthly Notices of the Royal Astronomical Society, 442, 1157-1165 (2014).

[49] Güdel, M. & Nazé, Y., “X-ray Spectroscopy of Stars,” The Astronomy & Astrophysics Review, 17, 309-408 (2009).

[50] Feigelson, E. et al., “X-ray Properties of Young Stars and Stellar Clusters,” Proc. Protostars and Planets V, 313-328 (2007).

[51] Dupree, A.K. et al., “TW Hya: Spectral Variability, X-rays, and Accretion Diagnostics,” The Astrophysical Journal, 750, 73 (2012).

[52] Güdel, M. & Telleschi, A., “The X-ray Soft Excess in Classical T-Tauri Stars,” Astronomy & Astrophysics, 474, L25-L28 (2007).

[53] Dupree, A.K. et al., “Structure and Dynamics of The Accretion Process and Wind In TW Hya,” The Astrophysical Journal, 789, 27 (2014).

[54] Cranmer, S.R., “Testing Models of Accretion-Driven Coronal Heating and Stellar Wind Acceleration for T-Tauri Stars,” The Astrophysical Journal, 706, 824-843 (2009).

[55] Tinetti, G. et al., “Infrared Transmission Spectra for Extrasolar Giant Planets,” The Astrophysical Journal, 654, L99-L102 (2007).

[56] Poppenhaeger, K., Schmitt, J.H.M.M., & Wolk, S.J., “Transit Observations of the Hot Jupiter HD 189733b at X-ray Wavelengths,” The Astrophysical Journal, 773, 62 (2013).

[57] Brickhouse, N.S. et al., “A Deep *Chandra* X-ray Spectrum of the Accreting Young Star TW Hydrae,” The Astrophysical Journal, 710, 1835-1847 (2010).

[58] Brickhouse, N.S. et al., “X-ray Determination of the Variable Rate of Mass Accretion onto TW Hydrae,” The Astrophysical Journal, 760, L21 (2012).

[59] Cirtain, J.W. et al., “Energy Release in the Solar Corona from Spatially Resolved Magnetic Braids.,” Nature, 493, 501-3 (2013).

[60] Cargill, P.J. & Klimchuk, J.A., “Nanoflare Heating of the Corona Revisited,” The Astrophysical Journal, 605, 911-920 (2004).

[61] Asgari-Targhi, M. et al., “The Spatial and Temporal Dependence of Coronal Heating by Alfvén Wave Turbulence,” The Astrophysical Journal, 773, 111 (2013).

[62] Brickhouse, N.S. et al., “Coronal Structure and Abundances of Capella from Simultaneous EUVE and ASCA Spectroscopy,” The Astrophysical Journal, 530, 387-402 (2000).

[63] Testa, P., Peres, G., & Reale, F., “Emission Measure Distribution in Loops Impulsively Heated at the Footpoints,” The Astrophysical Journal, 622, 695-703 (2005).

[64] Doschek, G.A., “Soft X-ray Spectroscopy of Solar Flares - an Overview,” The Astrophysical Journal Supplement Series, 73, 117 (1990).

[65] Canizares, C.R. et al., “High-Resolution X-ray Spectra of Capella: Initial Results from the *Chandra* High-Energy Transmission Grating Spectrometer,” The Astrophysical Journal, 539, L41-L44 (2000).

[66] Lemen, J.R. et al., “Coronal Activity in F-, G-, and K-Type Stars. III - The Coronal Differential Emission Measure Distribution of Capella, Sigma-Squared CrB, and Procyon,” The Astrophysical Journal, 341, 474 (1989).

[67] Cohen, D.H. et al., “Measuring The Shock-Heating Rate in the Winds of O Stars Using X-ray Line Spectra,” Monthly Notices of the Royal Astronomical Society, 444, 3729-3737 (2014).

[68] Hamann, W.R., "Stellar Winds from Hot Low-Mass Stars," Astrophys. Space Sci., 329, 151-158 (2010).

[69] Hirschi, R., “The Impact of Reduced Mass Loss Rates on the Evolution of Massive Stars,” Proc. of Clumping Hot-Star Winds Workshop, 9 (2008).

[70] Owocki, S.P. & Cohen, D.H., “X-ray Line Profiles from Parameterized Emission within an Accelerating Stellar Wind,” The Astrophysical Journal, 559, 1108-1116 (2001).

[71] Oskinova, L.M., Feldmeier, A., & Hamann, W.R., “High-Resolution X-ray Spectroscopy of Bright O-Type Stars,” Monthly Notices of the Royal Astronomical Society, 372, 313-326 (2006).

[72] Leutenegger, M.A. et al., “Constraints on Porosity and Mass Loss in O-Star Winds from the Modeling of X-ray Emission Line Profile Shapes,” The Astrophysical Journal, 770, 80 (2013).

[73] Ignace, R. et al., "X-ray Emission Line Profiles from Wind Clump Bow Shocks in Massive Stars," The Astrophysical Journal, 750, 40 (2012).

[74] Zhekov, S.A. et al., "*Chandra* LETG Observations of Supernova Remnant 1987a," The Astrophysical Journal, 645, 293-302 (2006).

[75] Heng, K. et al., "Probing Elemental Abundances in SNR 1987a Using *XMM-Newton*," The Astrophysical Journal, 676, 361-370 (2008).

[76] Dwek, E. et al., "Infrared and X-Ray Evidence for Circumstellar Grain Destruction by the Blast Wave of Supernova 1987a," The Astrophysical Journal, 676, 1029-1039 (2008).

[77] Draine, B.T. & Fraisse, A.A., "Polarized Far-Infrared and Submillimeter Emission from Interstellar Dust," The Astrophysical Journal, 696, 1 (2009).

[78] Draine, B.T. & Hensely, B., "Magnetic Nanoparticles In The Interstellar Medium: Emission Spectrum And Polarization," The Astrophysical Journal, 765, 159 (2013).